Food Chemistry: X 25 (2025) 102137

Contents lists available at ScienceDirect

Food Chemistry: X

journal homepage: www.sciencedirect.com/journal/food-chemistry-x

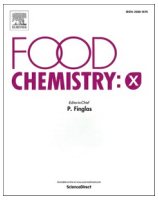

Effects of different white nanomaterials on pH response ability and physicochemical performance of anthocyanin-loaded carboxymethyl cellulose-polyvinyl alcohol films

Yuqian Li [a], Xue Yang [a], Yunfei Zou [a], Huixuan Zhang [a], Ying Zhou [a], Qiujin Zhu [a], Yuanyuan Liu [a,*], Zhengcong Wang [b,*]

[a] School of Liquor and Food Engineering, Guizhou University, Guiyang 550025, PR China
[b] College of Economics and Management, Huazhong Agricultural University, Wuhan, Hubei 430070, PR China

ARTICLE INFO

Keywords:
Anthocyanin-loaded film
pH-responsive
Performance improvement
Nanoparticles
Smart packaging

ABSTRACT

The anthocyanin-loaded films based on natural polymers as pH-responsive indicator are widely applied in the food preservation. However, the low mechanical strength and storage stability limited their practical application, there is an urgent demand to improve the performance of anthocyanin-loaded films. In order to avoid affecting the color indication of anthocyanins, we explored the effect of eight kinds of white nanomaterials on improving the performance of films. The results revealed that some nanomaterials showed capability in improving the polymer molecular interactions and enhancement in mechanical properties, barrier ability, and antioxidant activity. However, nanomaterials containing Zn was not suitable for anthocyanin-loaded film modification, because it could destroy the pH responsiveness of anthocyanin. The nano Al_2O_3 could increase the sensitivity of anthocyanin-loaded film in pH-response, which achieved the highest performance score during pork storage. This investigation will provide theoretical support for the development of more optimized pH-responsive anthocyanin-loaded films in the future.

1. Introduction

Foods are the essential foods for daily lives, and the quality and safety of meats reflect crucial influences with the development of living conditions. Therefore, the development of biodegradable intelligent packaging films for freshness testing of meat products is crucial in extending the shelf life of food. Recently, intelligent fresh preservation films with various activities have been developed and applied in food industry. For instance, the pH-responsive films with color indicator function could react with metabolites from food and undergo specific color changes in the form of gas sensors. These pH-responsive freshness indicators embedded in polymer films could monitor the internal environment of protein-based food packaging during shelf life, as well as differentiating changes in food freshness. It provides convenient information for consumers and food manufacturers and improves food safety. Additionally, common chemical colorimetric indicators, such as bromophenol blue, bromocresol green, bromocresol purple, and methyl red, may volatilize toxic substances and contaminate food, thereby harming human health (Xiao et al., 2023). Thus, it is impendency to develop natural pH-responsive color change substances for meat preservation.

Anthocyanins, natural plant flavonoid polyphenol of water-soluble pigments, are widely distributed in plant-based food (Alappat & Alappat, 2020). The basic structure of anthocyanins (3,5,7-trihydroxy-2-phenylbenzopyran) (Demirdöven, Karabiyikli, Tokatli, & Öncül, 2015) would contribute to the effective eliminate free radical properties, revealing promising development about food packaging. Additionally, as the pH sensitivity characteristic of anthocyanins, the changes of anthocyanin molecular structure would exhibit different colors under different pH buffer solutions. Therefore, anthocyanins are always selected as candidates for pH-responsive color indicator in food packaging application (Moradi, Tajik, Almasi, Forough, & Ezati, 2019). However, the low stability towards chromogeny and antioxidant leads to low effect in the process of meat preservation, reflecting the necessary in combining anthocyanins with other substances to compensate stability. As reported, proteins and polysaccharides with excellent film-forming capability could be used to improve the stability of anthocyanins (Park & Zhao, 2004).

Currently, films prepared from proteins and polysaccharides as film-

* Corresponding authors.
E-mail addresses: yyliu3@gzu.edu.cn (Y. Liu), zhengcong_wang@mail.hzau.edu.cn (Z. Wang).

https://doi.org/10.1016/j.fochx.2024.102137
Received 4 November 2024; Received in revised form 4 December 2024; Accepted 26 December 2024
Available online 28 December 2024

forming matrices such as chitosan (CS), carboxymethyl cellulose (CMC), sodium alginate (SA) and gelatin (Gel), exhibit an excellent moisture retention, biocompatibility, antimicrobial properties, film-forming ability, and easy degradability (Lu et al., 2019), revealing as common materials for film coating preparation. However, the weak mechanical strength and storage stability of degradable films made from polysaccharides and proteins limit the practical applications in the food industry. To address these limitations, the incorporation of nanomaterials has been shown to enhance the physical and chemical properties of polymer materials, including mechanical strength, water resistance, and gas barrier properties (Liao, Zhou, Hou, Zhang, & Huang, 2023). In the context of anthocyanin-loaded pH-responsive films, the color of nanomaterials, which can be influenced by strong light interference effects, may impact the color-indicating effect of the films. Anthocyanins are known to form chelates with metal ions, leading to a hyperchromic effect and a subsequent change in color (Sigurdson, Robbins, Collins, & Giusti, 2016). Thus, it is essential to explore nanomaterials that not only improve the performance of degradable films based on polysaccharides or proteins, but also maintain potential pH-responsive color indicating functionality.

Therefore, this study demonstrated the mechanical strength, pH-responsiveness, color sensitivity and stability of 4 film-forming materials loaded with equal amounts of anthocyanins (CS-P, SA-P, CMC—P, and Gel—P) to select out the suitable film-forming matrix. Then, in order to avoid the color of the nanomaterial itself affecting the color rendering effect of the indicator film, 8 white nanomaterials were chosen as modifiers for the anthocyanin-loaded films, including ZIF-8, cellulose nanofibers (CNF), nano-alumina (Al_2O_3), nano-silica (SiO_2), nano-titanium dioxide (TiO_2), nano-zinc oxide (ZnO), kaolin clay (NKL), and hydroxyapatite (HAP). It revealed the effects of various nanomaterials on the performance of pH-responsive color indicator films loaded with anthocyanins. It would provide guidance for the feasibility of enhancing the performance of natural biomolecular food packaging films with a color display function through the nanomaterials-addition.

2. Materials and methods

2.1. Materials

Sodium alginate (F.W. = (198.11) n, n = 80–750), CS (Mn 60–80 kDa, degree of deacetylation ≥85 %), CMC (CMC with viscosity of 1000–1400 mPa•s), polyvinyl alcohol (PVA with a degree of polymerization (DP) of 1750 ± 50, content ≥99 %) and Gel (animal source, alkaline gelatin, bloom strength~240 g bloom) were purchased from Sinopharm Chemical Reagent Co., Ltd. (Shanghai, China). Blueberry anthocyanin was purchased from Shaanxi Huike Plant Development Co. Ltd. (Shaanxi, China). ZIF-8 was synthesized according to the method of Jian (Jian et al., 2015) and the detailed method was applied as supporting documents (S1). Nano-TiO_2 (average particle size: 40 nm), nano-Al_2O_3 (α-phase Al_2O_3, particle size: 30 nm), nano-ZnO (average particle size: 50 nm), nano-HAP (average particle size: 60 nm) and nano-NKL (average particle size: 2.5 μm) were purchased from Macklin Reagent Co. Ltd. (Shanghai, China). CNF (content 1.20 %) were purchased from ScienceK Ltd. (Zhejiang, China). 1,1-diphenyl-2-picryl-hydrazyl radical (DPPH) were provided by Xilong Science Co. Ltd. (Guangzhou, China). Glycerol and acetic acid were obtained from Chengdu Chemical Reagent Co. Ltd. (Sichuan, China). All reagents were analytically pure.

2.2. Effect of different nanomaterials on anthocyanin discoloration

The 2 mL of 0.15 %, 1.50 % different nanomaterial solution and 8 mL 0.50 % anthocyanin solution were mixed. The above liquids were mixed with buffers of pH 2, 4, 6, 7, 8, 10, 12 at a ratio of 4:1, respectively. The color changes were recorded by taking photos.

2.3. Preparation of composite films

(1) Preparation of composite films.

The CS/PVA/anthocyanin composite films (CS-P) were prepared using solvent evaporation method (Hafsa et al., 2016). The film solution was prepared by dissolving 0.60 g CS into 28 mL acetic acid solution (1 %, *v*/v) at 40 °C for 1 h with magnetic stirrer. Then 0.40 g PVA was dispersed in 18 mL distilled water with a magnetic stirrer and stirred at 90 °C for 1 h. After mixed, 0.50 mL glycerin was added and stirred at 40 °C for 30 min with a magnetic stirrer. The 5 % (*w*/*v*) anthocyanin solution was prepared, 4 mL was sucked into CMC/PVA solution after filtration, and stirred for 30 min. After degassing, 25 mL of the film forming solution was poured into a petri dish to smooth the flow, and dried at 40 °C to form the film. CMC—P, Gel-P and SA-P composite membranes were prepared by according to the CS-P preparation. In the preparation process, CMC, Gel and SA were dissolved with equal amounts of distilled water instead of acetic acid solution.

(2) Preparation of nano-doped film.

Nano-doped films was prepared by referring to the preparation method of composite films. Distilled water and CMC were uniformly dissolved at 40 °C for 1 h with a magnetic stirrer to prepare 2 % (*w*/*v*) film forming solution. Then, PVA was dispersed in distilled water using a magnetic stirrer at 90 °C for 1 h to prepare 4 % (*w*/*v*) film forming solution. Subsequently, these were combined with 0.25 mL glycerin and stirred at 40 °C for 30 min with a magnetic stirrer. Anthocyanin (5 %, w/v, 2 mL) solution was added to CMC/PVA solution after filtration, and 0.69 % (w/v) nanomaterial dispersion was prepared. Then 3.60 mL nanomaterial dispersion was added to CMC/PVA solution and stirred for 30 min. The film forming solution was degassed and poured into the culture dish to smooth the flow, and dried to form a film at 40 °C. Other nanocomposite films were prepared with reference to the above methods. The actual concentration of nanomaterials in the preparation process should be consistent.

2.4. Determination of pH-sensitive property of film

The pH-sensitive property of film was measured according to the previous method (X. C. Wang et al., 2019). The film sample (1.50 cm × 1.50 cm) was immersed in a buffer solution at pH 2, 4, 6, 7, 8, 10, 12 for 15 min. Then, the appearance of the membrane sample was photographed under the same light source. The color parameters of the sample were determined using the color extractor software of mobile phone. Then the pH response sensitivity (ΔS/ΔE) of the film was calculated according to the to the following equations:

$$\Delta R = R_a - R_b\# \quad (1)$$

$$\Delta G = G_a - G_b\# \quad (2)$$

$$\Delta B = B_a - B_b\# \quad (3)$$

$$\Delta S = \sqrt{\Delta R^2 + \Delta G^2 + \Delta B^2}\# \quad (4)$$

$$\Delta L = L_a - L_b\# \quad (5)$$

$$\Delta A = A_a - A_b\# \quad (6)$$

$$\Delta B = B_a - B_b\# \quad (7)$$

$$\Delta E = \sqrt{\Delta L^2 + \Delta A^2 + \Delta B^2}\# \quad (8)$$

where R_a, G_a, B_a were the initial values of the red, green and blue; R_b, G_b, B_b were the gray values after storage. L_a, A_a and B_a were the color parameters of initial values, and L_b, A_b and B_b were the color parameters of film sample.

2.5. Reaction of films to ammonia and acetic acid

When detecting the freshness of meat, the volatile gas produced by meat can cause the change of environmental pH and affect the color of the indicator film. Response of composite films to volatile ammonia was tested according to previous study with some modifications. The film (20 × 20 mm) was suspended into 3 cm above the ice acetic acid and ammonia water with the volume fraction of 1 %, 10 % and 100 %. At 10 s, 20 s, 30 s, 60 s, 2 min, 5 min, 15 min and 30 min, the photos were taken under the same light source and the color parameters of the samples were determined. Then the pH response sensitivity (ΔS/ΔE) of the film was calculated according to the to the equations of 2.4.

2.6. Color stability

The color stability determination of composite film was improved based on Junjun Zhang's method (Zhang et al., 2019). The 1.50 × 1.50 film samples were placed under the same environmental conditions (25 °C) with 75 % humidity, photographed under the same light source every 24 h. The color parameters of the samples were determined by the color extraction software. The stability of the composite film was characterized by the total change rate of the three components of the RGB value of the film, according to the formula in 2.4 part.

2.7. Characterization of composite films

The test sample (dry sample) was fixed to the copper plate holder using a conductive adhesive and was sprayed with gold under vacuum conditions. Use a field emission scanning electron microscope (S-4800, Hitachi High-Technologies Corporation, Japan) to observe the microscopic morphology of the sample and take photographs (Liu et al., 2023). The Nexus 470 Fourier Transform Infrared Spectrometer (Nexus 470 Nicolet Co. Ltd., USA) was used to measure the infrared spectra of different composite films with a scanning range of 4000–400 cm^{-1} at room temperature, repeating 64 times. The X-ray diffractometer (Bruker D8 Advance Bruker GmbH, Germany) was applied to measure the diffraction patterns of the sample in the range of diffraction angle 2θ = 5–50° (Yuanyuan Liu et al., 2023). The measurement voltage was 40 kV, with continuous step scanning and a step size of 0.02°. After drying, the film was prepared into fragments and the thermal stability of films were tested by a thermogravimetric analyzer (TG 2900, TA Instruments Co., Ltd., USA) under the following test conditions: nitrogen flow rate 100 mL/min, heating rate 10 °C/min, and detection temperature range 25–600 °C (Cheng et al., 2024).

2.8. Mechanical properties

The tensile strength and elongation at break of the films were measured using a texture analyzer (CT3, Brookfield Instruments Co., Ltd., USA) according to Wang (Wang et al., 2024). Before test, the films were cut into rectangular strips (70 mm × 10 mm), and the thickness was measured and recorded using a thickness gauge. The initial grip separation was set to 40 mm and the stretching speed was set to 1 mm/s, with 0.05 N trigger point load. Each sample was analyzed for five times. The values of TS and EBA were calculated according to equations:

$$TS(MPa) = \frac{F(N)}{Thickness(mm) \times width(mm)}\# \quad (9)$$

$$EAB(\%) = \frac{L - L_0}{L_0} \times 100\# \quad (10)$$

where the F was the maximum load on the films during the tensile test in Newton (N). Thickness and width were the initial values of the films in millimeters (mm). L_0 (40 mm) was the test length of the films, which was the initial distance between the two fixtures and L (mm) was the length of the films at the time of fracture.

2.9. Water vapor barrier performance (WVP)

According to previous method, the film loaded with different nanomaterials was cut into 3 × 3 cm squares, 4 mL of distilled water was added to a glass bottle with a diameter of 1 cm and a depth of 4 cm, and the film was covered on the bottle (F. Liu et al., 2019) These bottles were placed in a dryer with dried silicone at 28 °C, creating a vapor pressure difference of 3692.50 Pa inside and outside the glass bottle. Record the weight changes of the bottle at the beginning (M_0) and the end (M_t). The water vapor permeability was calculated as follows:

$$WVP = \frac{(M_0 - M_t) \times L}{\text{Film area} \times T \times \Delta P}\# \quad (11)$$

ΔP(KPa) was the pressure difference inside and outside the glass bottle; L (mm) was the average thickness of the film; T(days) was the duration of the experiment.

2.10. Determination of the antioxidant ability of films

The DPPH was weighed and dissolved in anhydrous ethanol to achieve a concentration of 0.20 mmol/L. A certain amount of the films was weighed and submerged in 2 mL of the DPPH solution for 2 h. The light absorption value at 517 nm was recorded as A_1. The control group was mixed with anhydrous ethanol and DPPH solution, and the absorption value was recorded as A_0. The calculation formula was as follows:

$$\text{DPPH radical scavenging activity}(\%) = \frac{A_0 - A_1}{A_0} \times 100\%\# \quad (12)$$

2.11. Optical transmittance

Ultraviolet-visible spectrophotometer (UV-2700 Shimadzu Japan) was used to measure the transmittance of the films in the range of 200–800 nm. The film was cut into rectangular strips and placed in a quartz test tube. One end of the film was glued to the optical surface of the test tube and placed in the test pool. The blank test tube was paired as a control. The transmittance calculation formula:

$$O = \frac{Abs600}{T}\# \quad (13)$$

where Abs600 was the absorbance of the film at 600 nm. O was the opacity and T was the thickness of the film (mm).

2.12. Water solubility

To determine the water solubility of the film, the pre-weighed dry film sample (1.50 × 1.50 cm) was immersed in 30 mL ultra-pure water, placed at 25 ± 1 °C for 15 min, and the upper liquid was sucked up with an eyedropper. Insoluble ingredients were dried at 105 °C for 24 h to constant weight (W_1). Determination repeated 3 times, and the water solubility (S%) formula was as follows:

$$\text{Dissolutionrate} = \frac{W_0 - W_1}{W_0} \times 100\%\# \quad (14)$$

where W_0 was the initial film mass and W_1 was the mass of the insoluble component after soaking and drying.

2.13. Application of films for monitoring the freshness of pork

The response of composite membrane to pork was tested. Fill the petri dish with 10 g fresh pork sample and fix the films (10 × 10 mm) to the lid of the petri dish and seal it. At 25 °C, the image information of the film was captured by the mobile phone every 8 h (a total of 24 h).

2.14. Statistical analysis

All experiments were performed with 3 replications. All data were expressed as mean ± standard deviation (SD). One-way analysis of variance (ANOVA, SPSS software) was applied and significance analysis between experimental values was performed by Duncan's multiple comparison method ($P < 0.05$, SPSS software). Origin 2021 was used for graphing.

3. Results and discussion

3.1. Effect of various nanomaterials on responsiveness of anthocyanins

The color changes and absorption values of pure anthocyanin solutions at different pH were recorded (Fig. 1 a - b). The maximum absorption peak occurs at 514 nm under pH 2, indicating the predominant presence of anthocyanins in the form of flavonoid cations, which exhibit a purplish-red hue. Besides, leucoanthocyanins and pseudoalkaloids were produced at pH 4, leading to a dark red color. While the pH range of 6–8, anthocyanins mainly existed as blue quinone-type alkaloids, transitioning from red to blue. When the pH exceeded 8, anthocyanins formed as phenolic salts under alkaline conditions, gradually shifting from blue to yellow (Suthar & Saran, 2020). This was consistent with the previous study which the color of roselle anthocyanins/starch/polyvinyl alcohol composite film changed from red to yellow-brown as the increased pH (Zhang et al., 2019).

The color changes of anthocyanins and their corresponding light absorption values after adding 1.50 % of different nanomaterials were analyzed (Fig. 1 c and e). The addition of the nanomaterials ZIF-8 and ZnO resulted in color changes of anthocyanin solution observably (from purple red to yellowish brown). These specific nanomaterials shifted the solutions maximum absorption peak to 580 nm (Fig. 1 e), consistent with the observed shift towards a deep blue hue (Fig. 1 c). A similar phenomenon had been observed in sericin-anthocyanin-zinc nanocomplexes reported in previous study (Yao et al., 2022). The maximum absorption peaks of Al_2O_3 and TiO_2 also showed a redshift (Fig. 1 e), revealing the influence of anthocyanin color by Al_2O_3- and TiO_2-addition. The previous study also showed the phenomenon of high coloring effect between nanomaterial and anthocyanin mixture (Pereira, Picciani, Calado, & Tonon, 2022). It demonstrated that the 4 kinds of nanomaterials (Al_2O_3, TiO_2, ZnO and ZIF-8) revealed similar modification effects on the anthocyanin-loaded membrane at 1.50 % nanomaterials concentration, and the absorption peaks are all redshifted.

The color changes of nanomaterials and anthocyanin solutions at different pH values, and the absorption rate of anthocyanin solutions added with different nanomaterials at the same pH value were showed in Fig. 1 d. As the pH value increased, the color of the anthocyanin aqueous solution mixed with CNF, Al_2O_3, SiO_2, ZnO, NKL, and HAP changed from pink to purple and yellow-green, in particular, the color change of Al_2O_3 was the most obviously among them. Solutions containing ZIF-8 and TiO_2 showed minimal color changes with the increasing of pH, remaining brown and purple, respectively. The change in pH results in a significant shift in the maximum absorption peak of ZIF-8 (Fig. 1 f). At pH of 2–6 and 8–12, the difference in the maximum absorption peak of ZIF-8 decreased, indicating that the little color difference of the solution added with ZIF-8 at different pH values. In addition, the maximum absorption peak of Al_2O_3 at pH 7–8 underwent the obvious blue shift (from 500 nm to 600 nm), indicating that it could increase the sensitivity of anthocyanins to pH changes. Meanwhile, TiO_2 had a significant ($P < 0.05$) effect on the coloration of anthocyanins (Fig. 1 f). Under similar pH conditions, there was a significant ($P < 0.05$) difference in the peak position (shifted towards long wavelengths) compared to pure anthocyanins. Supplementary Fig. S1 showed the light absorption values of the same nanomaterial (1.50 %) at different pH values. The addition of ZIF-8, TiO_2, and ZnO caused obvious changed in the light absorption values compared with pure anthocyanins, resulting in similar changes between peaks in different pH ranges. Therefore, the addition of ZIF-8, ZnO and TiO_2 could affect the pH responsiveness of anthocyanins and thus affected their application in pH-responsive films.

3.2. The pH responsiveness of blending film with different matrix

pH sensitivity was a crucial property in intelligent packaging films, enabling the monitoring of food freshness through pH changes induced by food spoilage. The blending films with different polymers displayed distinct colors towards varying pH levels (Fig. 2), demonstrating their effective pH responsiveness. All four composite films showed a transition from red to blue to yellow as the pH increased.

The pH-responsive films were utilized for preserving and labeling meat products as indicators. The pH of fresh meat typically fell between 5 and 6, but during decay, the release of amine substances elevated the pH from 7 to 8. Thus, the rangeability of ΔE and ΔS values of the LAB colorimetric and RGB colorimetric methods, respectively, were selected for comparison investigation of pH-responsive accuracy of the films (Fig. 2 b – c). Furthermore, assessing the difference in pH change between pH 6 and pH 8 was beneficial for identifying films with high sensitivity in application of meat storage. Overall, changes in ΔS were greater than that in ΔE within significance. For example, at a pH of 8, the ΔE value of SA was 27.60 and the ΔS value was 109.19 (Fig. 2 b - c, $P < 0.05$). Previous studies also proved that the larger the change value, the more responsive the membrane was. The ratio of the value of ΔS (or ΔE) at pH 8 to pH 6 could provide insight into the differences in color change within this pH range. As Fig. 2 d illustrated, the S8/S6 value for SA-P (2.36) and CMC-P (2.63) blending films was higher than the E8/E6 value (1.98 and 1.91), while the opposite trend was observed for CS-P (4.02 of S8/S6 and 4.95 of E8/E6) and Gel-P films (0.42 of S8/S6 and 0.69 of E8/E6). This suggested that ΔS was appropriate for assessing color changes in SA-P and CMC-P films, whereas ΔE was suitable for evaluating color changes in CS-P and Gel-P films. Given the consistent relationship between ΔS and ΔE for the same blending film, future experiments would utilize ΔS as the primary metric to evaluate color changes in the films.

3.3. Response to volatile ammonia and acetic acid

The color sensitivity of pH-responsive films was essential for practical applications. During muscle protein degradation, volatile compounds like ammonia, amines, and sulfides were produced. Volatile nitrogen substances, particularly ammonia, could elevate the pH of muscle food, impacting its quality. Gas sensors' efficacy was assessed by observing color changes in blended films when exposed to ammonia and acid vapor. The color of the film changes obviously in acetic acid and ammonia water (Fig. 2 e and g). In ammonium hydroxide, color of films shifted from purple to blue and then to yellow-green, with Gel-P displaying the quickest transformation and highest sensitivity to ammonia gas within 20 s among samples (Fig. 2 f). In acetic acid, films tended to reddish-purple, with Gel-P exhibiting the vivid color change and large ΔS value fluctuation, increasing from 0 % to 83.46 % ($P < 0.05$), followed by CMC-P (Fig. 2 h). Overall, all films exhibited strong sensitivity to acidic and alkaline conditions, with Gel-P being sensitive and CS-P showing less pronounced color variations.

3.4. Color stability of blending film with different matrix during storage

The color change of pH-responsive films was dependent on the structural stability of anthocyanins, which was influenced by their interaction with various polymer matrices. The level of stability played a crucial role in determining the longevity of pH-responsive films in practical applications. This study showed that CMC-P had the smallest change trend in ΔS values within 10 days at room temperature (Fig. 2 i - j). In Yanglin Wu's study, lower color changes during storage of CMC-P were also observed (Wu & Li, 2022). The ΔS values of Gel—P, SA-P and

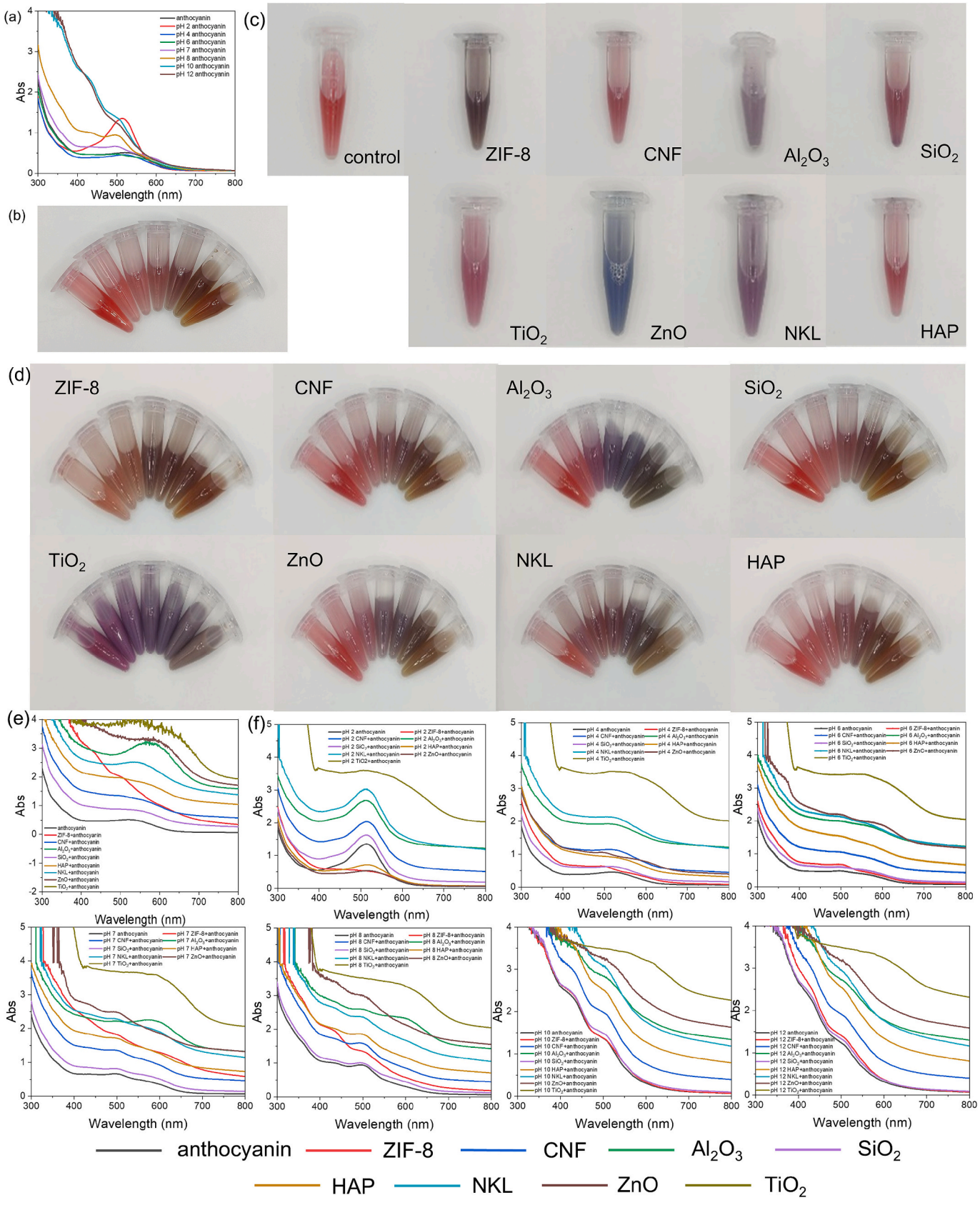

Fig. 1. UV–vis spectra (a) and colors (b) of anthocyanin at different pH, color changes (c) and absorbance (e) of anthocyanin solution after adding different nanomaterials, color changes (d) of anthocyanin solution with different nanomaterials at different pH and the anthocyanin absorbance (f) of different nanomaterials at the same pH.

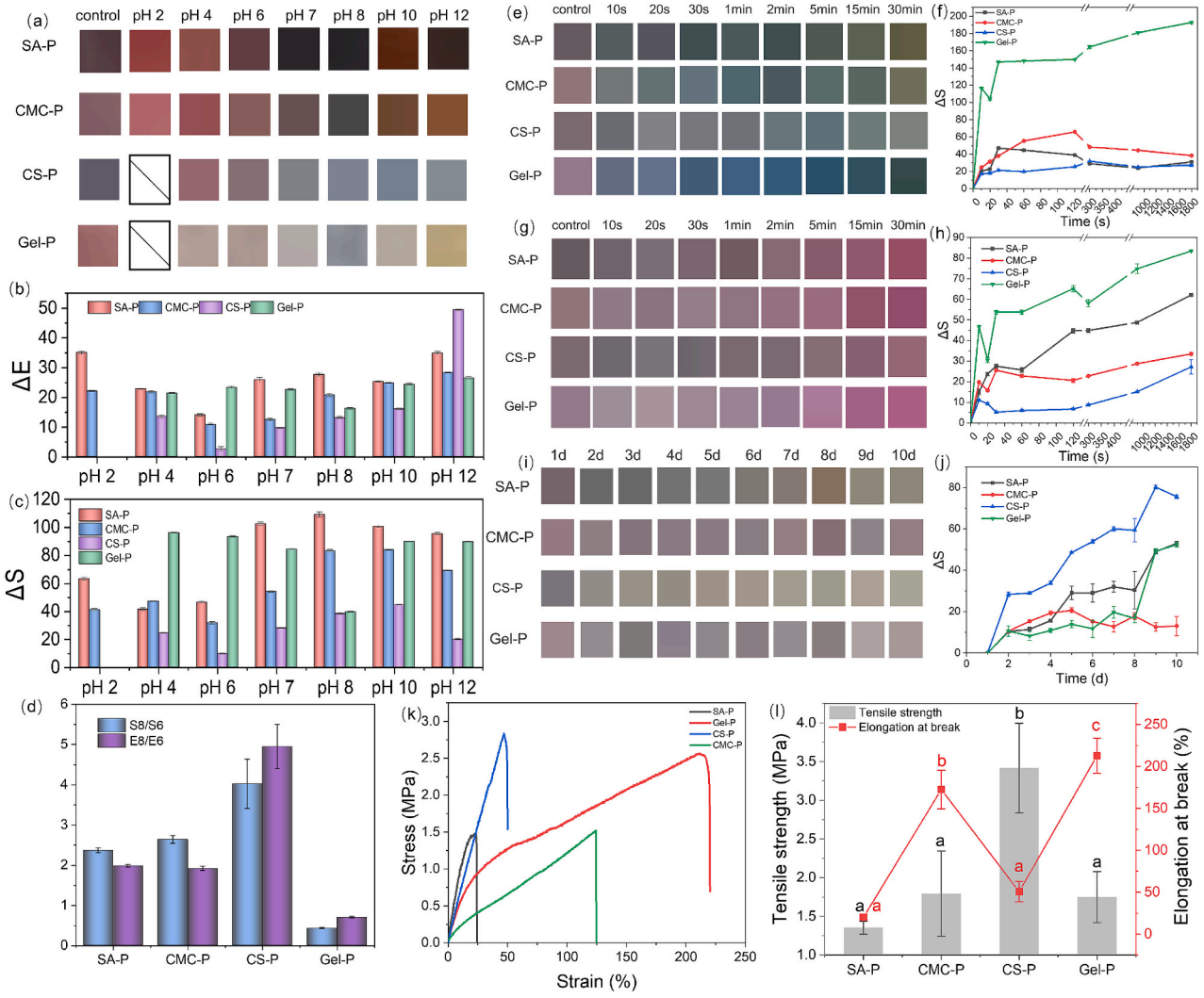

Fig. 2. Color changes of films after being immersed in different buffer solutions (a), color values including ΔE (b), ΔS (c) and their ratios at pH 8 and pH 6 (d), colors and ΔS values in ammonia (e, f) and acetic acid (g, h). The stability of the film at room temperature (i, j), stress-strain curve (k), tensile strength and elongation at break (l) of composite film. Different lowercase letters in the figure indicate significantly different ($P < 0.05$).

CS-P were 52.41, 53.00 and 75.57, respectively, showing a significant ($P < 0.05$) increasing trend. Previous studies have also observed the color changes of the three composite films during storage. These findings suggested that the color stability of CMC-P films was superior, indicating effective protection of anthocyanins within the CMC film and preventing oxidation.

3.5. Mechanical strength of blending film with different matrix

The stress-strain curve, elongation at break, and tensile strength of the composite film were showed in Fig. 2 k - l. The SA-P film demonstrated low mechanical strength of 1.35 MPa, while Gel-P and CMC-P films showed strengths of 1.75 MPa and 1.79 MPa, respectively. Notably, the CS-P film exhibited the highest tensile strength of 3.42 MPa among samples within significance ($P < 0.05$). This could be attributed to the increased intermolecular forces between chitosan and PVA molecules, which might limit polymer chain movement and enhance film rigidity (Ghorpade, Dias, Mali, & Mulla, 2019).

Comparing the elongation at break, Gel-P revealed the highest elongation of 212.71 %, followed by CMC-P of 172.42 %. Although the CS-P film revealed high tensile strength, its stiffness increased and elongation at break decreased. In comparison, the tensile strength and elongation at break of the SA-P film were the lowest (1.35 MPa and 20.06 %), which might be due to the decreased compatibility with PVA molecules. By evaluating the pH responsiveness, color stability and mechanical properties of 4 different polymer matrices (CMC—P) including CMC, Gel, PVA and SA, it was concluded that the CMC-P showed minimal ΔS variation in storage stability, indicating the excellent storage stability. Besides, CMC-P also revealed excellent sensitivity and mechanical properties. Therefore, CMC-P blend film was selected for further research.

3.6. pH responsiveness of various nanomaterials loaded CMC-P films

Films containing different nanomaterials showed obvious color changes at different pH values (Fig. 3 a). The initial color of the films containing ZIF-8 and ZnO changed to yellow in obvious, which was different from the initial purplish red color of CMC—P. In particular, at different pH values, the color changes of ZnO and ZIF-8 groups were less obvious than that of the other composite films loaded with nanomaterials, indicating the reduced response of anthocyanins towards pH. Moreover, Al^{3+} formed a stable nanocomposite with anthocyanins after ionization, making the initial blue color of Al_2O_3-supplementary films (Estévez, Otero, & Mosquera, 2011). However, the color change of Al_2O_3 at different pH was still be seen from purple red to blue, which indicated that the initial color change showed no influence on the pH response.

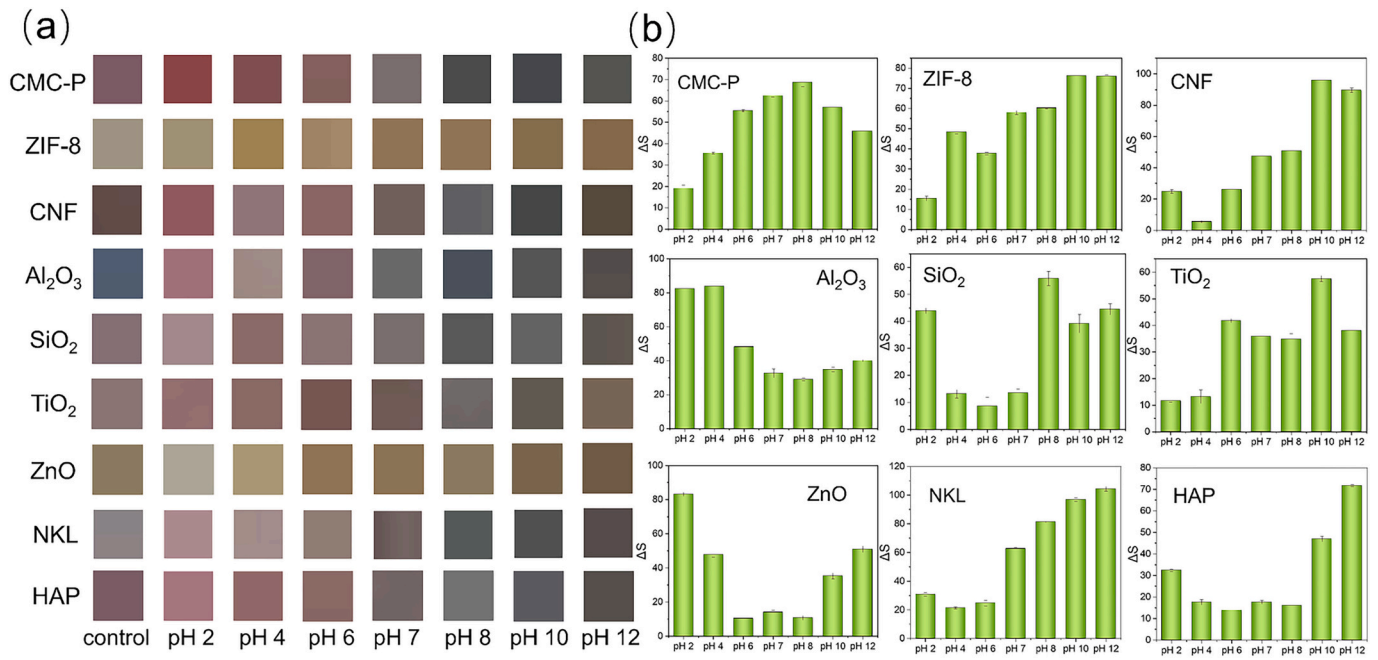

Fig. 3. Color changes (a) and ΔS values (b) of composite films at different pH.

The initial color of the films with other nanomaterials did not change significantly, and showed similar color changes to CMC-P at different pH (from bright red to yellowish brown), and still had good pH response ability.

Except for Al_2O_3 and ZnO, ΔS values of composite films in alkaline environment (pH 10–12) are higher than those in acidic environment (Fig. 3 b), indicating that the color changes of composite films in alkaline environment were more obvious than those under acidic environment, revealing the high sensitivity of films towards alkaline conditions. For instance, the obvious responses of CNF were observed as changing from purple red to yellow brown in alkaline environments and from purple red to deep red in acidic environments. In the acidic environment (pH 2), the ΔS values of Al_2O_3 and ZnO were the highest as 82.43 and 83.15 in respective, affected by the initial color. In comparation, it proved the higher responsiveness to acidic environment towards Al_2O_3 and ZnO, and the response of Al_2O_3 was stronger.

3.7. Color sensitivity of various nanomaterials loaded CMC-P films

The pH sensitivity was a key factor for smart packaging. As the color change and ΔS curve showed, It could be seen from the color changes and ΔS curves that under alkaline conditions (ammonia solution, Fig. 4

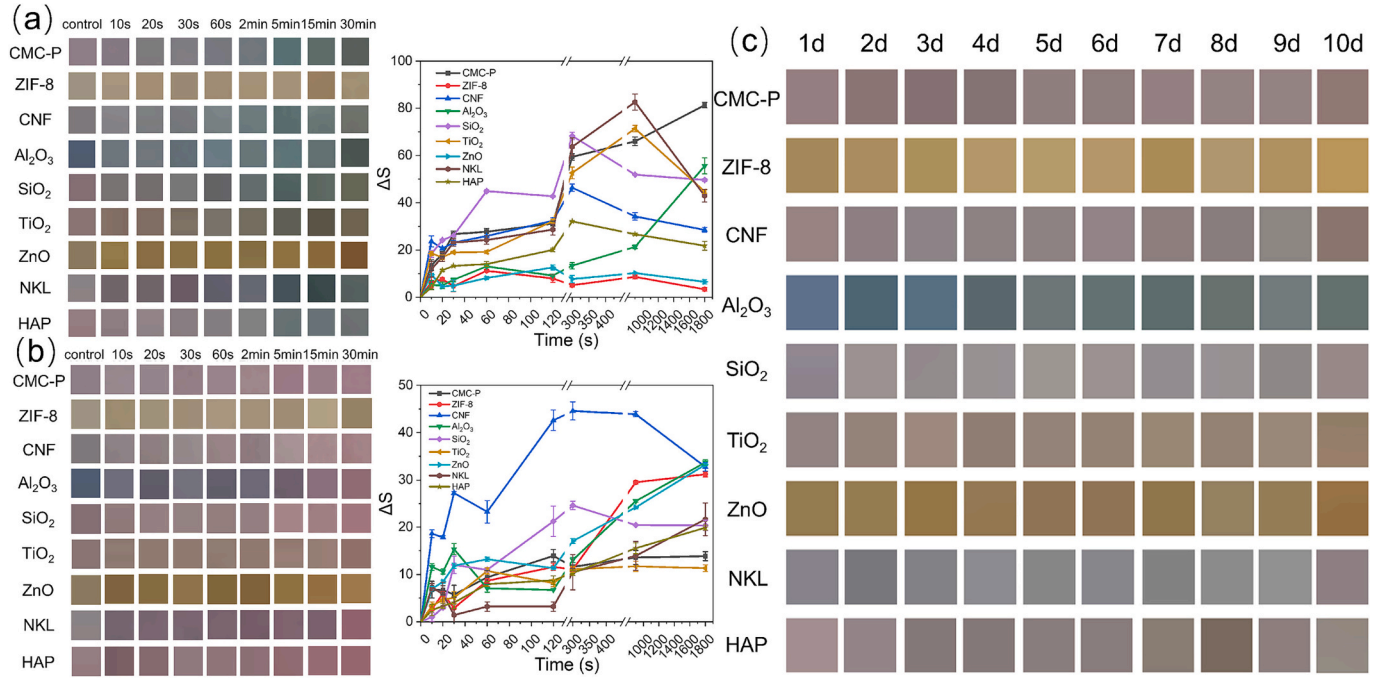

Fig. 4. Color changes and ΔS values of the composite films loaded with different nanomaterials exposed to ammonia (a) and acetic acid (b), color changes during the storage period of the composite films (c).

a), the films containing ZIF-8 and ZnO had no obvious color changes, and the ΔS value had no change trend, which proved that the ZIF-8 and ZnO contained films failed in color sensitivity under alkaline conditions. Consistent with the pH response, although the initial blue color of Al_2O_3, the ΔS curve showed a significant ($P < 0.05$) increase under alkaline induction (from 0 to 55.59), indicating that the initial color did not affect the color sensitivity of the composite film. Films containing NKL and TiO_2 showed higher sensitivity on the ΔS curve under alkaline conditions in comparation with others films, which was influenced by the hyperchromic effect generated between the nanomaterial and anthocyanins. Specifically, after the exposure of $NH_3{\cdot}H_2O$, the color changed from purple to yellow-gray, following as the fluctuation of pH and the increased concentration of quinone and chalcone alkaloids. Under acidic conditions, the color change of ZIF-8 and ZnO films was not obvious (from purple to raspberry red). Apart from these two, the ΔS of composite membranes loaded with other nanomaterials increased under acidic conditions, especially CNF (increased to 32.75) and Al_2O_3 (increased to 33.70) within significance ($P < 0.05$). It indicated that CNF, Al_2O_3 and other nanomaterials could improve the sensitivity of anthocyanin-loaded membranes under acidic conditions.

3.8. Color stability of various nanomaterials loaded CMC-P films during storage

Meat freshness testing using composite films relied on color change, implying the critical of film stability. The color changes of different composite films at 25 °C were observed (Fig. 4 c). It showed that the color stability of the indicator film loaded by all nanomaterials did not change significantly during the storage period, indicating that the addition of nanomaterials will not affect the storage stability of the composite film. This could be proved by previous research that anthocyanins would be degraded slowly under temperature below 60 °C (Araujo-Díaz, Leyva-Porras, Aguirre-Bañuelos, Álvarez-Salas, & Saavedra-Leos, 2017).

3.9. Characterization of various nanomaterials loaded CMC-P films

SEM was used to analyze the distribution of nanomaterials inside and on the surface of CMC-P blends (Fig. 5 a). The CMC-P film without nanomaterials showed a smooth, flat and uniform surface morphology. After adding various nanomaterials, the composite film of CNF, Al_2O_3,

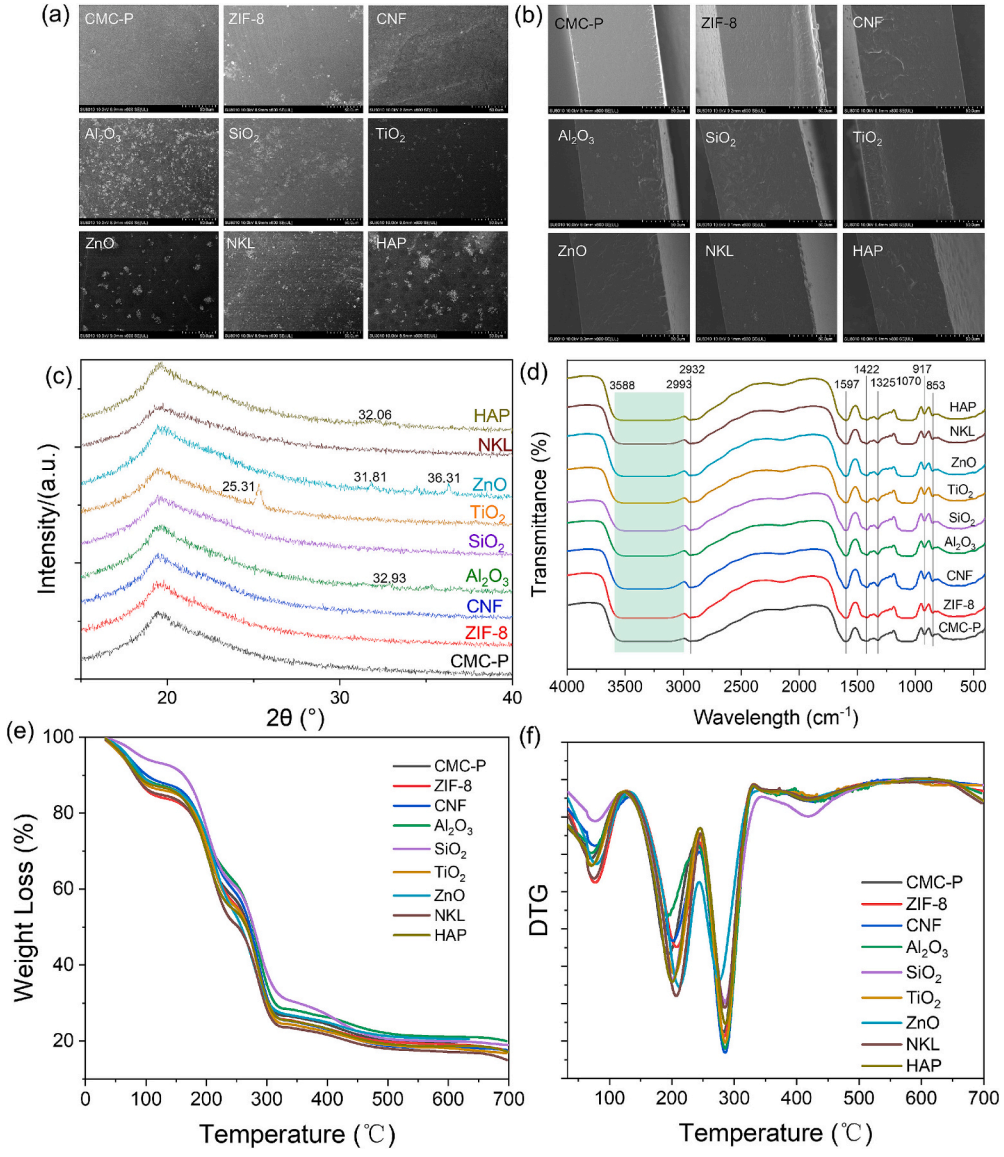

Fig. 5. SEM micrographs of the surface (a) and cross sections (b) of the indicating films. XRD (c), FTIR spectra (d), TGA (e) and DTG (f) curves of composite films loaded with different nanomaterials.

SiO_2, TiO_2, and NKL revealed an obvious particle structure, uniform dispersion, consistent particle size, with no phase separation phenomenon. The interconnection of CNF, Al_2O_3, SiO_2, TiO_2, and NKL within films promoted the formation of intermolecular hydrogen bonds between the nanomaterials and the film-forming matrix, forming the permeable network. The cross-section of the CMC-P film without nanomaterials was smooth and free of cracks and pores. However, compared with the CMC-P film, all parts of the composite film doped with nanomaterials exhibited a relatively rough structure. The composite film with added nanomaterials showed uniform distribution of fillers in the polymer matrix, indicating strong compatibility between the nanofillers and the polymer matrix in the anthocyanin-loaded film. This indicated the possibility of hydrogen bonding between the components. Moreover, SEM images showed no obvious aggregation or phase separation of the nanomaterials, confirming their uniform distribution in the CMC/PVA mixture.

The FTIR spectrum analysis of the CMC-P composite film revealed a broad peak at 3588–2993 cm^{-1}, contributing by the stretching vibration of O—H (Cheng et al., 2024). The peak at 2932 cm^{-1} was associated with the stretching vibration of CH groups in the biopolymer chains (X. Qin et al., 2024). Peak at 1422 cm^{-1} was assigned to the symmetric carboxyl group in CMC (el Miri et al., 2015), while the peak at 1070 cm^{-1} was corresponded to the stretching vibration of C-O-C in the hexagonal ring structure of CMC. Peaks detected at 1608 and 1325 cm^{-1} were corresponded to the stretching vibrations of C═C aromatic ring and phenolic C—O angle deformation (Kang et al., 2018).

The peak at 3588 cm^{-1} in Fig. 5 d was caused by the stretching vibration of the hydroxyl group in the PVA, a phenomenon also reported before (Zhu et al., 2020). The broad peak observed between 3588 and 2993 cm^{-1} in the composite film was attributed to the stretching vibration of free hydroxyl groups, aligning with the spectral peaks of PVA and CMC films. This suggested that there was no chemical reaction between PVA and CMC. Compared to the CMC-P film, no significant changes were generated by functional groups in nano-composite films, implying the stable chemical structure of CMC-P with the filler addition.

The XRD analysis was used to investigate the crystal structure and compatibility of films (Fig. 5 c). Previously, it highlighted that CMC was a common amorphous polymer displaying a broad diffraction peak around 20°. Consequently, any peaks observed in the diffraction pattern could be attributed to the polymer PVA and its corresponding characteristic peaks (el Naggar et al., 2022). The peaks observed at approximately 11.6°, 19.4°, 23.0°, and a small peak near 40.8° were attributed to the PVA crystal structure. Upon the addition of different nanoparticles, the composite film with HAP revealed a minor peak at $2\theta = 32.06°$, a characteristic peak of the HAP hexagonal phase. The film containing TiO_2 exhibited a small peak at 25.31°, a characteristic peak of the anatase phase of TiO_2, consistent with the previous result (Mariappan et al., 2022). The composite film with ZnO showed characteristic peaks at $2\theta = 31.81°$ and $2\theta = 36.31°$, while the film containing Al_2O_3 exhibited a broad Al_2O_3 characteristic peak at $2\theta = 35.34°$ (Akkaya Arıer & Tepehan, 2014). This showed that the Al_2O_3 tend to aggregate and crystallize in the film matrix, indicating lower compatibility compared to other nanoparticles. However, no obvious peak broadening changes or new sharp peaks were observed in the composite film, indicating that nanoparticles-addition showed no influence on the structure of the film matrix. Additionally, it suggested that these nanoparticles were well dispersed within CMC and PVA molecules through interactions.

The thermal stability of the polymer blends was investigated by analyzing the thermogravimetric data and corresponding differential thermogravimetric (DTG) curves of multiple membranes when heated under a N_2 atmosphere. There were 4 different weight loss plateaus among all samples (Fig. 5 e). The initial weight loss process of the TGA showed a relative low rate (6.71–15.95 %) of mass loss, which might be due to the evaporation of residual bound water in film (Fig. 5 f). The subsequent weight loss process (24.57–33.88 %) was mainly attributed to the thermal degradation of CMC, decomposition of methylcellulose, decarboxylation of CMC functional groups leading to CO_2 loss, as well as cleavage/dehydration reactions within the CMC structure (Yuanyuan Liu, Zhang, et al., 2023). The third weight loss process (25.80–33.72 %) was the primary thermal degradation of polyvinyl alcohol (PVA), stemming from the decomposition of polymer chains into volatile fragments. The final weight loss process (4.06–10.34 %) was due to the interaction between CMC and PVA molecules and the relative stiffness of the CMC chains, resulting in restricted movement of the PVA chains, thereby increasing the decomposition temperature and improved thermal stability of the film.

Based on DTG curve analysis, the CMC-P film exhibited an endothermic peak at 194.28 °C, whereas in comparation, other nanocomposite films displayed higher endothermic peaks ranging from 195.29 to 210.49 °C during the second weight loss stage. In the third weight loss stage, the CMC-P film showed an endothermic peak at 282.45 °C, while in comparation, other nanocomposite films exhibited higher endothermic peaks between 283.46 and 285.49 °C. This phenomenon might be influenced by the interaction between the nanomaterials and CMC/PVA. The molecular interaction reduced the mobility of the polymer chains, leading to a slow heat penetration into the internal structure, consequently enhancing the heat resistance of the composite film.

3.10. Mechanical properties of various nanomaterials loaded CMC-P films

Fig. 6 a, b, and c showed the stress-strain curve, elongation at break, and tensile strength of the composite film, respectively. Factors such as the chemical structure and size of the nanofillers, the compatibility with the polymer matrix, and the concentration of the nanofillers affected the mechanical properties of nanocomposite films (Oun & Rhim, 2017). After adding nanomaterials, the tensile strength of the composite film was significantly ($P < 0.05$) improved. Specifically, ZnO composite film showed the highest tensile strength of 10.63 MPa compared with other films, followed by Al_2O_3(7.63 MPa), NKL (7.74 MPa) and CNF (5.56 MPa). The improvement was mainly attributed to interfacial adhesion between nanoparticles and polymers, which enhanced intermolecular interactions such as hydrogen bonds and restricted the motion of molecular chains. This was supported by the increased heat resistance observed in the composite film following the addition of nanomaterials in TGA, as well as the uniform dispersion of nanomaterials in the composite film as shown in SEM.

The high tensile strength of the ZnO composite film might be influenced by the incorporation of high modulus ZnO nanoparticles into the CMC/PVA matrix. This would improve the aggregation state of the film and enhance the interaction (such as B. Van der Waals force) between CMC/PVA molecules and ZnO nanoparticles. It contributed to the film's ability to resist the movement of molecular segments under the influence of external forces. Additionally, the heterogeneous nucleation effect of nano-zinc oxide particles increased the crystallinity of polymer macromolecules, thereby improving the mechanical properties of the film.

The SiO_2 composite film showed the high EAB value (183.62 %), indicating the effective effect of SiO_2 on increasing the flexibility of film (Fig b). Generally, films with higher tensile strength revealed lower EAB values (Yaofa Liu et al., 2019). The TS values of ZnO, NKL, Al_2O_3 and CNF composite films were significantly ($P < 0.05$) increased by 5.93-fold, 4.31-fold, 4.26-fold and 3.10-fold, while the EAB values were significantly ($P < 0.05$) decreased by 2.13-fold, 1.46-fold, 1.29-fold and 1.28-fold in comparation with CMC—P. This was associated with the weak hydrogen bonds between CMC and PVA molecules, as well as the new hydrogen bonds formed between the nanomaterials and polymers. As proved by the previous study, the new bonds would prevent the molecules from moving, making the film exhibited educed elasticity when it was broke (X. Liu et al., 2019).

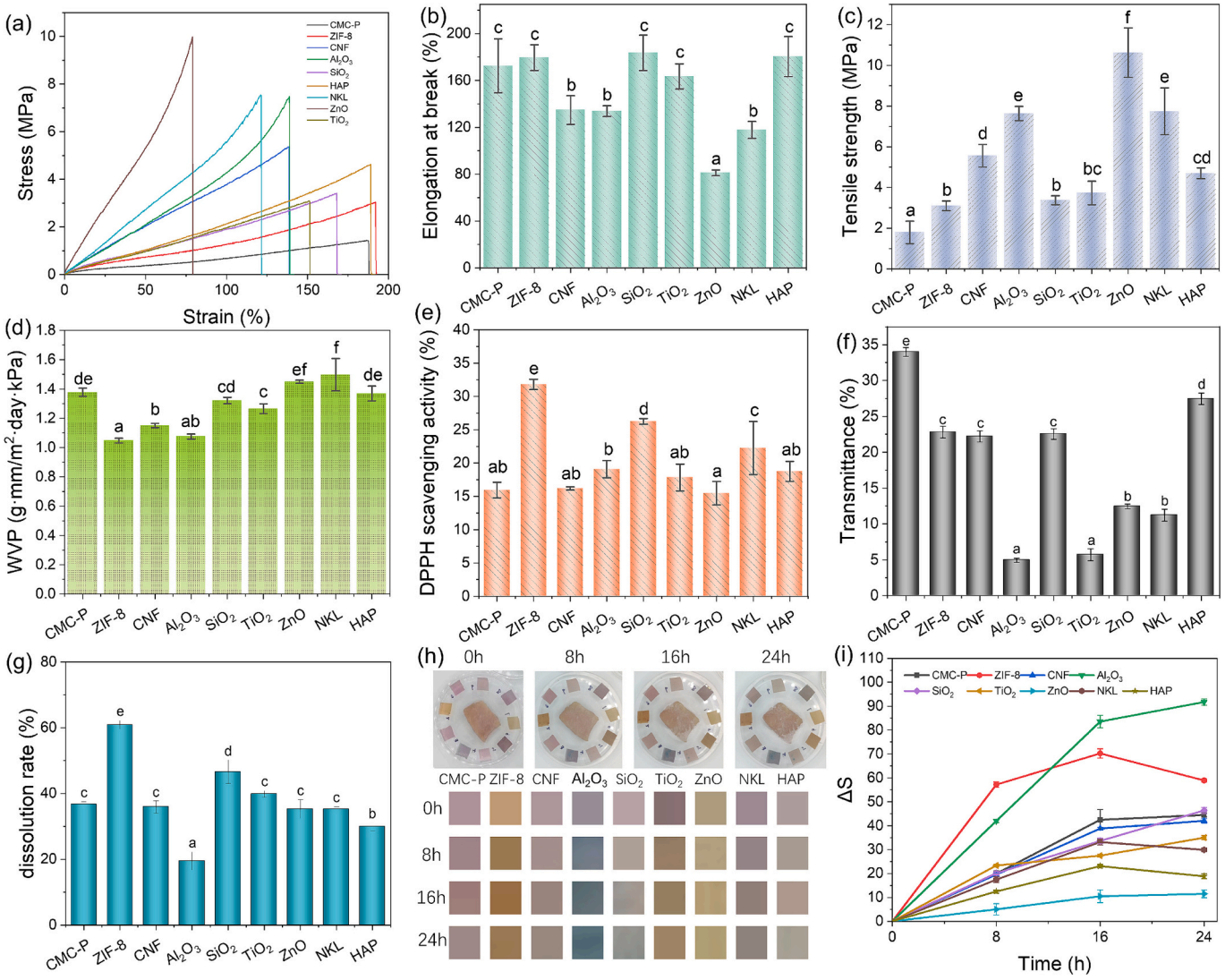

Fig. 6. Stress-strain curve (a), elongation at break (b), tensile strength (c), water vapor transmittance (d), antioxidant activity (e), light transmittance (f), solubility (g) of composite films loaded with different nanomaterials, the color changes of films during the storage of pork sample at 25 °C for 24 h (h), and the corresponding change of ΔE of the indicating films (i). Different lowercase letters in the figure indicate significantly different ($P < 0.05$).

3.11. WVP of different nanomaterials loaded CMC-P films

It revealed that the WVP value of CMC-P was 1.38 g·mm/m^2·day·kPa, which was the highest among the other composite films (Fig. 6 d). This was attributed to the presence of numerous hydroxyl groups in CMC, which enhanced the affinity for water molecules. Compared with CMC-P (1.38 g·mm/m^2·day·kPa), the addition of ZIF-8, CNF, Al_2O_3 and TiO_2 reduced the WVP value to 1.05, 1.15, 1.08 and 1.27 g·mm/m^2·day·kPa, respectively ($P < 0.05$). The formation of additional intermolecular hydrogen bonds between the nanoparticles and the CMC matrix reduced the availability of hydrophilic groups to interact with water molecules inside and outside the film matrix, for which the moisture-proof properties were improved. In addition, the reduction of WVP was related to the spatial structure of the film. Nanoparticles were integrated into the film matrix to form a "curved path" for water molecules to pass through, hindering molecular exchange and increasing the barrier effect of the film (Gasti et al., 2022). Nanoparticles densified the composite film denser and effectively prevented the diffusion of water molecules. The WVP of the composite film with ZnO and NKL increased slightly, since the addition of nanomaterials to form pores on the surface of the composite film, increased the channel of external water molecules, and reduced the barrier property of the film. It was consistent with previous studies on SEM that the nanoparticles accumulated on the surface of the film and formed pores. Thus, it could be proved that composite films modulated with NKL and ZnO would reduce the barrier properties.

3.12. Antioxidant ability of various nanomaterials loaded CMC-P films

The DPPH free radical scavenging rate of the composite membrane was determined to evaluate the antioxidant capacity (Fig. 6 e). Phenolic flavanols with strong antioxidant activity in anthocyanins led to a high DPPH free radical scavenging rate scavenging rate of 15.94 % in CMC-P film. The antioxidant activity of the composite films containing Al_2O_3 (19.07 %), NKL (22.27 %), SiO_2 (26.24 %) and ZIF-8 (31.80 %) was significantly ($P < 0.05$) higher than that of the control films (15.94 %). Consistent with the present study, the Al_2O_3-added enhanced the antioxidant effect than before in that of grapefruit peel extract (Bokhary et al., 2022). The increased antioxidant activity by Al_2O_3 might be triggered by the strong intrinsic antioxidant capacity of Al_2O_3. Additionally, for SiO_2 film, the clearance rate of 22.27 % could be attributed to the adsorption of free radicals by SiO_2 nanoparticles (Jabraili, Pirsa, Pirouzifard, & Amiri, 2021). According to previous research (Saroha, Khan, Raghuvanshi, & Dutt, 2022), the antioxidant activity of NKL was

mainly related to antioxidant properties in supporting polyphenols during adsorption and film formation. The antioxidant activity of ZIF-8 was related to metal coordination, which reduced the redox potential of the ligand, thereby increasing the antioxidant activity of flavonoids and anthocyanins (Kasprzak, Erxleben, & Ochocki, 2015).

3.13. Optical transmittance of various nanomaterials loaded CMC-P films

The transmittance of the composite film was measured by ultraviolet spectrophotometer (Fig. 6 f). It was observed that the light transmittance of the nine composite films was less than 35 %, which might associate with the presence of anthocyanins with the characteristic of improving UV-blocking properties. The addition of anthocyanins significantly ($P < 0.05$) improved the light-blocking performance of the film, and similar results were also obtained in the previous study (Lu, Zhou, Yu, Chen, & Yuan, 2022).

Among films, the CMC-P film revealed the highest light transmittance as 33.97 % (Fig. 6 f). However, the decreased degrees of transmission loss were demonstrated with the different nanoparticles added. In particular, the addition of Al_2O_3, TiO_2 and ZnO significantly ($P < 0.05$) reduced the light transmittance of the composite film to 4.96 %, 5.72 % and 12.46 %, which was attributed to the light scattering and shielding effects produced by the large specific surface area of the nanoparticles. Adding nanoparticles or colored groups (such as C—C or C—O) to anthocyanins would reduce the transparency and light transmittance of the film.

3.14. Water solubility of various nanomaterials loaded CMC-P films

The water resistance of the composite film was evaluated by measuring the dissolution rate (Fig. 6 g). In comparation with the dissolution rate of CMC-P film (36.64 %), the incorporation of Al_2O_3 and HAP significantly ($P < 0.05$) reduced the dissolution rate to 17.19 % and 6.70 % in respective, attributing to the strong interaction between nanofillers and biopolymers. Therefore, the interaction between CMC-PVA polymer chains and nanoparticles would limit the motion of the polymer chains, probably resulting in a reduced dissolution rate of the polymer in the nanocomposite. The similar results were also showed when alginate films were combined with nano-fillers (H. Wang et al., 2019). However, the addition of ZIF-8 and SiO_2 significantly ($P < 0.05$) improved the dissolution rate of the composite film to 60.84 % and 46.61 %, respectively. This would contribute to the presence of hydrophilic silanol groups on the surface of nano-SiO_2 particles as well as the penetrative water molecules by porous structure of ZIF-8 (Zhuang et al., 2014).

3.15. Application of films for monitoring the freshness of pork

To evaluate pork freshness, the usage of anthocyanin-based smart packaging films was demonstrated (Fig. 6 h - i). Composite films containing different nanomaterials exhibited different color changes over time. Among them, the Al_2O_3-modified film revealed the highest sensitivity of 91.72, followed by SiO_2 (46.38) and TiO_2 (34.99) films. Within 24 h, as the pH value increased, Al_2O_3 changed from purple to dark blue, SiO_2 turned to blue-gray, and TiO_2 turned to brown-yellow (Fig. 6 h). These were associated with the action of bacteria and fungi on meat proteins, which broke down to form volatile nitrogen-containing compounds such as ammonia and amines (Zhang et al., 2019). In contrast, ZIF-8 and ZnO composite films exhibited no obvious color changes during the same period, indicating low sensitivity. It was consistent with ammonia response (Fig. 4 a) that ZIF-8 and ZnO also reduced the sensitivity of composite films.

4. Conclusion

In this study, polyvinyl alcohol mixed with chitosan, sodium alginate, sodium carboxymethyl cellulose and gelatin was used as the film-forming polymer, while anthocyanins were used as the pH response color indicator to construct a pH response intelligent colorimetric film. Based on pH response, color sensitivity, mechanical properties and storage stability, the CMC-P with excellent comprehensive performance was selected for the investigation of influence of nanomaterials. The results showed that the addition of nanomaterials significantly improved the thermal stability and mechanical properties of CMC-P films, while maintaining the stability of chemical structure. However, zinc-containing nanomaterials are unfavorable to the color indication of anthocyanin indicator films. Overall, alumina performed best in barrier properties, water resistance and tensile strength, and significantly improved pH response when storing pork. Therefore, this study analyzed the pH response performance of different white nanomaterials modified anthocyanin-supported films, making up for the shortcomings of existing studies and providing a reference for the future development of more optimized anthocyanin-supported films. While the current study demonstrates the potential for applications of this smart film in food packaging, its mass production still faces some challenges. A significant concern is ensuring the safety and compatibility of nanomaterials used in these films, particularly in food contact applications. In future studies, a key area for future exploration is the development of active nanomaterials that not only boost the sensitivity of anthocyanin-based color changes but also possess antimicrobial properties. Such materials could significantly enhance the overall performance of the films. Additionally, further research is needed to investigate how to maintain the processing stability of anthocyanins during large-scale production. Moreover, optimizing the performance of anthocyanin-loaded films in practical long-term storage and application scenarios is essential for their broader implementation.

CRediT authorship contribution statement

Yuqian Li: Writing – original draft, Methodology, Investigation, Formal analysis, Data curation. **Xue Yang:** Validation, Investigation, Data curation. **Yunfei Zou:** Investigation, Formal analysis. **Huixuan Zhang:** Validation, Investigation, Data curation. **Ying Zhou:** Data curation. **Qiujin Zhu:** Writing – review & editing, Methodology. **Yuanyuan Liu:** Writing – review & editing, Supervision, Project administration, Formal analysis, Conceptualization. **Zhengcong Wang:** Writing – review & editing, Conceptualization.

Declaration of competing interest

The authors declare that they have no known competing financial interests or personal relationships that could have appeared to influence the work reported in this paper.

Acknowledgments

This work was financially supported by the Guizhou Provincial Basic Research Key Program (Natural Science) (No. ZK [2024] 015), the National Natural Science Foundation of China (No.32360594), the Cultivation Project of Guizhou University (No. [2020] 36), and the Fundamental Research Funds for the Central Universities (Program No. 2662022ZKQD003).

Appendix A. Supplementary data

Supplementary data to this article can be found online at https://doi.org/10.1016/j.fochx.2024.102137.

Data availability

The authors do not have permission to share data.

References

Akkaya Arıer, U. O., & Tepehan, F. Z. (2014). Influence of Al_2O_3:TiO_2 ratio on the structural and optical properties of TiO_2–Al_2O_3 nano-composite films produced by sol gel method. *Composites Part B: Engineering, 58*, 147–151. https://doi.org/10.1016/j.compositesb.2013.10.023

Alappat, B., & Alappat, J. (2020). Anthocyanin pigments: Beyond aesthetics. *Molecules, 25*(23), 5500. https://doi.org/10.3390/molecules25235500

Araujo-Díaz, S. B., Leyva-Porras, C., Aguirre-Bañuelos, P., Álvarez-Salas, C., & Saavedra-Leos, Z. (2017). Evaluation of the physical properties and conservation of the antioxidants content, employing inulin and maltodextrin in the spray drying of blueberry juice. *Carbohydrate Polymers, 167*, 317–325. https://doi.org/10.1016/j.carbpol.2017.03.065

Bokhary, K. A., Maqsood, F., Amina, M., Aldarwesh, A., Mofty, H. K., & Al-yousef, H. M. (2022). Grapefruit extract-mediated fabrication of photosensitive aluminum oxide nanoparticle and their antioxidant and anti-inflammatory potential. *Nanomaterials, 12*(11), 1885. https://doi.org/10.3390/nano12111885

Cheng, Y., Xu, J., Zhang, R., Lin, J., Zhou, M., Qin, X., Wang, K., Zhou, Y., Zhu, Q., Jin, Y., & Liu, Y. (2024). Development of multi-cross-linking, rapid curing, and easy cleaning, edible hydrogels for meat preservation. *Food Hydrocolloids, 155*, Article 110186. https://doi.org/10.1016/j.foodhyd.2024.110186

Demirdöven, A., Karabiyikli, S., Tokatli, K., & Öncül, N. (2015). Inhibitory effects of red cabbage and sour cherry pomace anthocyanin extracts on food borne pathogens and their antioxidant properties. *LWT- Food Science and Technology, 63*(1), 8–13. https://doi.org/10.1016/j.lwt.2015.03.101

Estévez, L., Otero, N., & Mosquera, R. A. (2011). Molecular structure of cyanidin metal complexes: Al(III) versus mg(II). *Theoretical Chemistry Accounts, 128*(4–6), 485–495. https://doi.org/10.1007/s00214-010-0829-0

Gasti, T., Dixit, S., Hiremani, V. D., Chougale, R. B., Masti, S. P., Vootla, S. K., & Mudigoudra, B. S. (2022). Chitosan/pullulan based films incorporated with clove essential oil loaded chitosan-ZnO hybrid nanoparticles for active food packaging. *Carbohydrate Polymers, 277*, Article 118866. https://doi.org/10.1016/j.carbpol.2021.118866

Ghorpade, V. S., Dias, R. J., Mali, K. K., & Mulla, S. I. (2019). Citric acid crosslinked carboxymethylcellulose-polyvinyl alcohol hydrogel films for extended release of water soluble basic drugs. *Journal of Drug Delivery Science and Technology, 52*, 421–430. https://doi.org/10.1016/j.jddst.2019.05.013

Hafsa, J., Smach, M. A., Ben Khedher, M. R., Charfeddine, B., Limem, K., Majdoub, H., & Rouatbi, S. (2016). Physical, antioxidant and antimicrobial properties of chitosan films containing Eucalyptus globulus essential oil. *LWT- Food Science and Technology, 68*, 356–364. https://doi.org/10.1016/j.lwt.2015.12.050

Jabraili, A., Pirsa, S., Pirouzifard, M. K., & Amiri, S. (2021). Biodegradable nanocomposite film based on gluten/silica/calcium chloride: Physicochemical properties and bioactive compounds extraction capacity. *Journal of Polymers and the Environment, 29*(8), 2557–2571. https://doi.org/10.1007/s10924-021-02050-4

Jian, M. P., Liu, B., Liu, R. P., Qu, J. H., Wang, H. T., & Zhang, X. W. (2015). Water-based synthesis of zeolitic imidazolate framework-8 with high morphology level at room temperature. *RSC Advances, 5*(60), 48433–48441. https://doi.org/10.1039/C5RA04033G

Kang, S. L., Wang, H. L., Guo, M., Zhang, L. D., Chen, M. M., Jiang, S. W., … Jiang, S. T. (2018). Ethylene-vinyl alcohol copolymer-montmorillonite multilayer barrier film coated with mulberry anthocyanin for freshness monitoring. *Journal of Agricultural and Food Chemistry, 66*(50), 13268–13276. https://doi.org/10.1021/acs.jafc.8b05189

Kasprzak, M. M., Erxleben, A., & Ochocki, J. (2015). Properties and applications of flavonoid metal complexes. *RSC Advances, 5*(57), 45853–45877. https://doi.org/10.1039/C5RA05069C

Liao, J., Zhou, Y. H., Hou, B., Zhang, J. M., & Huang, H. H. (2023). Nano-chitin: Preparation strategies and food biopolymer film reinforcement and applications. *Carbohydrate Polymers, 305*, Article 120553. https://doi.org/10.1016/j.carbpol.2023.120553

Liu, F., Chan, W., Chen, M. S., Xu, F. F., Ma, J. G., & Zhong, F. (2019). Tailoring physicochemical properties of chitosan films and their protective effects on meat by varying drying temperature. *Carbohydrate Polymers, 212*, 150–159. https://doi.org/10.1016/j.carbpol.2023.120553

Liu, X., Chen, X., Ren, J., Chang, M., He, B., & Zhang, C. (2019). Effects of nano-ZnO and nano-SiO_2 particles on properties of PVA/xylan composite films. *International Journal of Biological Macromolecules, 132*, 978–986. https://doi.org/10.1016/j.ijbiomac.2019.03.088

Liu, Y., Liu, Y., Han, K., Cai, Y., Ma, M., Tong, Q., & Sheng, L. (2019). Effect of nano-TiO_2 on the physical, mechanical and optical properties of pullulan film. *Carbohydrate Polymers, 218*, 95–102. https://doi.org/10.1016/j.carbpol.2019.04.073

Liu, Y., Wang, K., Ma, J., Wang, Z., Zhu, Q., & Jin, Y. (2023). Effect of yolk spheres as a key histological structure on the morphology, character, and oral sensation of boiled egg yolk gel. *Food Chemistry, 424*, Article 136380. https://doi.org/10.1016/j.foodchem.2023.136380

Liu, Y., Zhang, Y., Zhen, M., Wu, Y., Ma, M., Cheng, Y., & Jin, Y. (2023). Effect of catechin and tannins on the structural and functional properties of sodium alginate/gelatin/ poly(vinylalcohol) blend films. *Food Hydrocolloids, 135*, Article 108141. https://doi.org/10.1016/j.foodhyd.2022.108141

Lu, M., Zhou, Q., Yu, H., Chen, X. E., & Yuan, G. F. (2022). Colorimetric indicator based on chitosan/gelatin with nano-ZnO and black peanut seed coat anthocyanins for application in intelligent packaging. *Food Research International, 160*, Article 111664. https://doi.org/10.1016/j.foodres.2022.111664

Lu, X., Chen, J. H., Guo, Z. B., Zheng, Y. F., Rea, M. C., Su, H., … Miao, S. (2019). Using polysaccharides for the enhancement of functionality of foods: A review. *Trends in Food Science & Technology, 86*, 311–327. https://doi.org/10.1016/j.tifs.2019.02.024

Mariappan, A., Pandi, P., Rajeswarapalanichamy, R., Neyvasagam, K., Sureshkumar, S., Gatasheh, M. K., & Hatamleh, A. A. (2022). Bandgap and visible-light-induced photocatalytic performance and dye degradation of silver doped HAp/TiO_2 nanocomposite by sol-gel method and its antimicrobial activity. *Environmental Research, 211*, Article 113079. https://doi.org/10.1016/j.envres.2022.113079

el Miri, N., Abdelouandi, K., Barakat, A., Zahouily, M., Fihri, A., Solhy, A., & el Achaby, M. (2015). Bio-nanocomposite films reinforced with cellulose nanocrystals: Rheology of film-forming solutions, transparency, water vapor barrier and tensile properties of films. *Carbohydrate Polymers, 129*, 156–167. https://doi.org/10.1016/j.carbpol.2015.04.051

Moradi, M., Tajik, H., Almasi, H., Forough, M., & Ezati, P. (2019). A novel pH-sensing indicator based on bacterial cellulose nanofibers and black carrot anthocyanins for monitoring fish freshness. *Carbohydrate Polymers, 222*, Article 115030. https://doi.org/10.1016/j.carbpol.2019.115030

el Naggar, A. M., Heiba, Z. K., Mohamed, M. B., Kamal, A. M., Lakshminarayana, G., & Abd-Elkader, O. H. (2022). Effect of MnS/ZnS nanocomposite on the structural, linear and nonlinear optical properties of PVA/CMC blended polymer. *Optical Materials, 128*, Article 112379. https://doi.org/10.1016/j.optmat.2022.112379

Oun, A. A., & Rhim, J.-W. (2017). Preparation of multifunctional chitin nanowhiskers/ZnO-ag NPs and their effect on the properties of carboxymethyl cellulose-based nanocomposite film. *Carbohydrate Polymers, 169*, 467–479. https://doi.org/10.1016/j.carbpol.2017.04.042

Park, S.-I., & Zhao, Y. (2004). Incorporation of a high concentration of mineral or vitamin into chitosan-based films. *Journal of Agricultural and Food Chemistry, 52*(7), 1933–1939. https://doi.org/10.1021/jf034612p

Pereira, P. F. M., Picciani, P. H. D., Calado, V., & Tonon, R. V. (2022). Anthocyanin-sensitized gelatin-ZnO nanocomposite based film for meat quality assessment. *Food Chemistry, 372*, Article 131228. https://doi.org/10.1016/j.foodchem.2021.131228

Qin, X., Cai, X., Wang, Y., Chen, L., Zhao, J., Zhang, Y., Bi, S., Zhou, Y., Zhu, Q., Cheng, Y., & Liu, Y. (2024). A water-resistant egg white/chitosan/pectin blending film with spherical-linear molecular interpenetrating network strengthened by multifunctional tannin-nisin nanoparticles. *International Journal of Biological Macromolecules, 277*, Article 134548. https://doi.org/10.1016/j.ijbiomac.2024.134548

Saroha, V., Khan, H., Raghuvanshi, S., & Dutt, D. (2022). Development of polyvinyl alcohol-based antioxidant nanocomposite films with nanokaolin impregnated with polyphenols from pomegranate peel extract. *Food Packaging and Shelf Life, 32*, Article 100848. https://doi.org/10.1016/j.fpsl.2022.100848

Sigurdson, G. T., Robbins, R. J., Collins, T. M., & Giusti, M. M. (2016). Evaluating the role of metal ions in the bathochromic and hyperchromic responses of cyanidin derivatives in acidic and alkaline pH. *Food Chemistry, 208*, 26–34. https://doi.org/10.1016/j.foodchem.2016.03.109

Suthar, M. K., & Saran, P. L. (2020). Anthocyanins from *Ocimum sanctum* L., a promising biomolecule for development of cost-effective and widely applicable pH indicator. *3. Biotech, 10*(9), 388. https://doi.org/10.1007/s13205-020-02380-5

Wang, H., Gong, X., Miao, Y., Guo, X., Liu, C., Fan, Y.-Y., Zhang, J., Niu, B., & Li, W. (2019). Preparation and characterization of multilayer films composed of chitosan, sodium alginate and carboxymethyl chitosan-ZnO nanoparticles. *Food Chemistry, 283*, 397–403. https://doi.org/10.1016/j.foodchem.2019.01.022

Wang, K., Li, C., Zhu, M., Zhang, W., Yuan, J., Liu, X., Ma, J., Wang, Z., Zhou, Y., Zhu, Q., Jin, Y., & Liu, Y. (2024). Redistribution and fusion of protein-lipid assemblies within the egg yolk sphere under slight non-destructive deformation causing a change in thermal gel properties. *Food Chemistry, 460*, Article 140577. https://doi.org/10.1016/j.foodchem.2024.140577

Wang, X. C., Yong, H. M., Gao, L., Li, L. L., Jin, M. J., & Liu, J. (2019). Preparation and characterization of antioxidant and pH-sensitive films based on chitosan and black soybean seed coat extract. *Food Hydrocolloids, 89*, 56–66. https://doi.org/10.1016/j.foodhyd.2018.10.019

Wu, Y., & Li, C. (2022). A smart film incorporating anthocyanins and tea polyphenols into sodium carboxymethyl cellulose/polyvinyl alcohol for application in mirror carp. *International Journal of Biological Macromolecules, 223*, 404–417. https://doi.org/10.1016/j.ijbiomac.2022.10.282

Xiao, Z. G., Han, L. N., Gu, M. Q., Zhu, Y. Q., Zhang, Y. F., Li, Z., … Lu, F. (2023). Performance comparison of anthocyanin-based smart indicator films. *Food Packaging and Shelf Life, 40*, Article 101187. https://doi.org/10.1016/j.fpsl.2023.101187

Yao, L., Hao, M. L., Zhao, F., Wang, Y. L., Zhou, Y. R., Liu, Z. Y., … Zhang, L. (2022). Fabrication of silk sericin-anthocyanin nanocoating for chelating and saturation-visualization detection of metal ions. *Nanoscale, 14*(46), 17277–17289. https://doi.org/10.1039/D2NR04047F

Zhang, J. J., Zou, X. B., Zhai, X. D., Huang, X. W., Jiang, C. P., & Holmes, M. (2019). Preparation of an intelligent pH film based on biodegradable polymers and roselle anthocyanins for monitoring pork freshness. *Food Chemistry, 272*, 306–312. https://doi.org/10.1016/j.foodchem.2018.08.041

Zhu, J. F., Li, Q. Y., Che, Y. C., Liu, X. C., Dong, C. C., Chen, X. Y., & Wang, C. (2020). Effect of Na_2CO_3 on the microstructure and macroscopic properties and mechanism analysis of PVA/CMC composite film. *Polymers, 12*(2), 453. https://doi.org/10.3390/polym12020453

Zhuang, J., Kuo, C.-H., Chou, L.-Y., Liu, D.-Y., Weerapana, E., & Tsung, C.-K. (2014). Optimized metal–organic-framework nanospheres for drug delivery: Evaluation of small-molecule encapsulation. *ACS Nano, 8*(3), 2812–2819. https://doi.org/10.1021/nn406590q